

# Using buoyant mass to measure the growth of single cells

Michel Godin<sup>1,6,7</sup>, Francisco Feijó Delgado<sup>1,7</sup>, Sungmin Son<sup>2</sup>, William H Grover<sup>1</sup>, Andrea K Bryan<sup>1</sup>, Amit Tzur<sup>3</sup>, Paul Jorgensen<sup>3,6</sup>, Kris Payer<sup>4</sup>, Alan D Grossman<sup>5</sup>, Marc W Kirschner<sup>3</sup> & Scott R Manalis<sup>1,2</sup>

**We used a suspended microchannel resonator (SMR) combined with picoliter-scale microfluidic control to measure buoyant mass and determine the ‘instantaneous’ growth rates of individual cells. The SMR measures mass with femtogram precision, allowing rapid determination of the growth rate in a fraction of a complete cell cycle. We found that for individual cells of *Bacillus subtilis*, *Escherichia coli*, *Saccharomyces cerevisiae* and mouse lymphoblasts, heavier cells grew faster than lighter cells.**

Understanding how the rate of cell growth changes during the cell cycle and in response to growth factors and other stimuli is of fundamental interest. Over the decades, various approaches have been developed for describing cellular growth patterns, but different studies have often reached irreconcilable conclusions, even for the same cell types. The debate has focused on whether cells grow at a constant rate (linear) or at a rate that is dependent on their size (exponential), although more complex growth curves have also been suggested. The mean dry mass accumulation of *E. coli* has been reported as increasing linearly<sup>1</sup>, and cell length growth has been described as bilinear<sup>2</sup>, bilinear and trilinear<sup>3</sup>, and exponential<sup>4</sup>. The size of the budding yeast *S. cerevisiae* has been observed to increase exponentially by some approaches<sup>5,6</sup>, but to have a nonexponential and cell cycle–dependent growth curve by others<sup>7</sup>. For mammalian cells, volume measurements have shown linear growth for rat Schwann cells<sup>8</sup> and exponential growth, with a varying rate constant, for mouse lymphoblast cells<sup>9</sup>. Several factors may contribute to the discrepancies between different growth models: (i) cells are minute, irregularly shaped objects; (ii) proliferating cells increase their size only by a factor of 2, so distinguishing between different cell growth models with mathematical rigor requires highly precise measurements; (iii) a wide variety of methods have been used to measure growth,

including approaches that average across populations as well as those that monitor individual cells; and (iv) a cell’s size includes both volume and mass, which can change at different rates.

Although both mass and volume are important parameters, mass is more fundamentally related to cell growth than is volume. Volume can change disproportionately to mass, thereby altering a cell’s density. In cells without rigid cell walls, volume can change rapidly in response to osmotic stresses, whereas even in cells with cell walls, the size of low-density intracellular vacuoles can change to alter the density of cells<sup>10</sup>. Fundamentally, cell growth is the creation of new biomass, the polymerization of small molecules into the lipids, proteins and RNA that make up the membrane, cytoplasm and organelles. But most research into cell size and growth has focused on volume, for lack of methods to measure the mass of individual cells.

An ideal method for measuring cell growth rates would directly and continuously monitor the mass and volume accumulation of single, unperturbed cells with high precision. In recent years, optical microscopy has been the closest match to this ideal<sup>3,5,11</sup>, but volume determination by microscopy has lacked sufficient precision to conclusively distinguish between cell growth models. Potential alternatives include using fluorescent protein reporters that are correlated with cell size<sup>5</sup> and using phase microscopy to measure dry mass during cell growth<sup>11</sup>. Here we describe a system that can precisely monitor the growth of single cells in terms of buoyant mass and show that bacteria, yeast and mammalian lymphoblast cells grow at a rate that is proportional to their buoyant mass. Buoyant mass is defined by  $m_{\text{buoyant}} = V(\rho_{\text{cell}} - \rho_{\text{fluid}})$ , where  $\rho$  is density and  $V$  is cell volume. It is dependent on the amount of biomass in the cell, most of which is denser than water, and so is analogous to the dry mass of the cell.

We developed a dynamic fluidic control system that enables the buoyant mass of cells as small as bacteria and as large as mammalian lymphocytes to be repeatedly measured with a suspended microchannel resonator (SMR). The SMR consists of a vacuum-packed, hollow microcantilever beam containing an embedded fluidic microchannel, and it is capable of weighing nanoparticles, bacterial cells and submonolayers of adsorbed proteins with femtogram resolution (1-Hz bandwidth)<sup>12</sup>. As individual cells transit the microchannel, a shift in the resonant frequency of the SMR is observed that corresponds to the buoyant mass of the cell. We implemented a feedback algorithm that reverses the direction of fluid flow upon detecting a cell transiting through the SMR, thereby reintroducing the cell into the cantilever (Fig. 1a,b). Continuously alternating flow direction creates a dynamic trap that allows for consecutive buoyant mass measurements of the

<sup>1</sup>Department of Biological Engineering and <sup>2</sup>Department of Mechanical Engineering, Massachusetts Institute of Technology, Cambridge, Massachusetts, USA.

<sup>3</sup>Department of Systems Biology, Harvard Medical School, Boston, Massachusetts, USA. <sup>4</sup>Microsystems Technology Laboratory and <sup>5</sup>Department of Biology, Massachusetts Institute of Technology, Cambridge, Massachusetts, USA. <sup>6</sup>Present addresses: Department of Physics, University of Ottawa, Ottawa, Ontario, Canada (M.G.); Donnelly Centre for Cellular and Biomolecular Research, University of Toronto, Toronto, Canada (P.J.). <sup>7</sup>These authors contributed equally to this work. Correspondence should be addressed to S.R.M. (scottm@media.mit.edu).

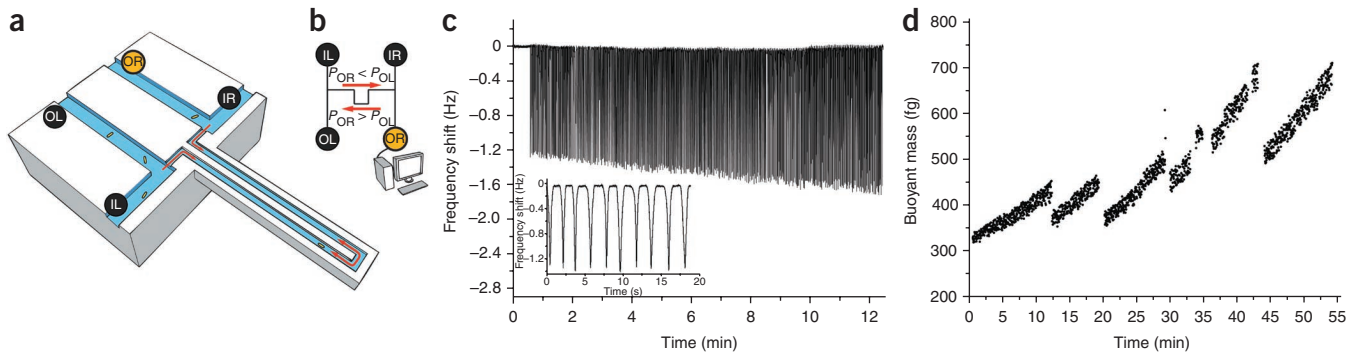


**Figure 1** | Dynamic trapping of single cells. **(a)** Illustration of the suspended microchannel resonator (SMR) trapping a single cell. Embedded channel cross-sections for bacteria, yeast and mammalian L1210 mouse lymphoblasts are  $3 \times 8 \mu\text{m}$ ,  $8 \times 8 \mu\text{m}$  and  $15 \times 20 \mu\text{m}$ , respectively. The silicon walls are opaque except in the  $15 \times 20\text{-}\mu\text{m}$  device, which has thinner walls. **(b)** Schematic of fluidics: sample is injected in parallel through the left and right inlets (IL and IR) and collected at the left and right outlets (OL and OR). While trapping, IL, IR and OL are kept at the same constant pressure; variable pressure at OR applied by a computer-controlled regulator determines the direction of fluid flow in the device. **(c)** Raw data showing 400 measurements of one *B. subtilis* cell's buoyant mass. The frequency shift increase with time indicates cellular growth. Inset, detail of a few peaks that show a locally stable baseline forms after each pass through the SMR, allowing for drift compensation. **(d)** Several *B. subtilis* cells were sequentially trapped. Each point represents the amplitude of the frequency shift, converted to buoyant mass, as the cell transits through the cantilever. Each set of points (for example, from 0 to 12 min) is one single cell or nonsegregated cells. Heavier cells have higher growth rates.

same cell. Because the cell fully exits the SMR before flow reversal, the baseline resonant frequency is acquired after each measurement, allowing compensation for drift arising from temperature variations or accretion on the walls of the microchannel. Dilute cultures of nonadherent cells in any desired growth medium can be loaded directly into the system.

The dynamic trap is very stable when measuring polystyrene particles that are less than half the size of the channel height ( $3\text{--}15 \mu\text{m}$ ). We trapped such particles for more than 20 h ( $>32,000$  measurements) (**Supplementary Fig. 1**). Sample concentration was the main limiting factor of the trapping duration. Low concentrations ( $\leq 10^7 \text{ ml}^{-1}$ ) decrease the probability of additional particles randomly drifting into the cantilever and becoming trapped along with the particle being measured. The maximal trapping duration for cells was typically shorter than for polystyrene particles and was dependent on the cell type. On average, *E. coli* and *B. subtilis* could be trapped for 500 s and 300 s, respectively, before being lost. Yeast and L1210 mouse lymphoblast cells could be trapped in excess of 30 min in a similar system as bacteria but with larger SMR channels. When living cells were trapped, growth was observed from the increasing amplitude of the resonant frequency peaks (**Fig. 1c**). Trapped cells are in an open system, as the suspended microchannel is in constant contact with the larger inlet and outlet channels (**Fig. 1a**), which act as reservoirs of nutrients. Diffusion and convection prevent local depletion of nutrients by the growing cell. Variability in the peak amplitudes (**Fig. 1c**) limits the precision of this method and is mainly due to the trapped cell taking different flow paths as it turns the corners at the cantilever tip. Different flow paths, as well as increased interaction with the microchannel walls, may also explain why cells with irregular shapes (for example, oblong *E. coli* and *B. subtilis*) escape the dynamic trap much more frequently than do polystyrene particles and round cells.

After conversion of resonant frequency shifts, growth could be observed as steadily increasing buoyant mass, as in a series of trapped *B. subtilis* cells (**Fig. 1d**). Occasionally, the magnitude of the frequency shifts would instantaneously drop by a factor of 2, suggesting that the trapped cell had divided into two daughter

cells, one of which had escaped the trap (**Supplementary Fig. 2**). Adding the poison sodium azide to a culture of *S. cerevisiae* continuously being loaded to the device resulted in a greatly diminished rate of increase in buoyant mass, demonstrating that these increases are indeed due to cell growth (**Supplementary Fig. 3**).

To determine whether growth rate depends on size, we used a method where the 'instantaneous' growth rate was measured by trapping a cell for a period much shorter than the cell's own life cycle. For each trapping event, a growth rate is determined and associated with the cell's buoyant mass at the start of the trapping event. By plotting the growth rate versus buoyant mass, we can piece together temporally localized growth rates of several individual cells to determine the size dependency of growth, provided that the measurement errors are below the natural variability. Such a plot does not necessarily depend on knowing the position of each cell in the cell-division cycle, although such information could be valuable and may be obtainable in future devices. We sampled cells from exponential-phase cultures of *B. subtilis*, *E. coli*, *S. cerevisiae* and L1210 mouse lymphoblasts. Growth rates for each cell were determined by performing linear fits to the buoyant mass data from each trapping event. We plotted growth rates against initial buoyant mass for *B. subtilis* (**Fig. 2a**), *E. coli* (**Fig. 2b**), *E. coli* grown at low temperature (**Supplementary Fig. 4**), *S. cerevisiae* (**Fig. 2c**) and L1210 mouse lymphoblasts (**Fig. 2d**). A clear trend is observable in all four cell types: heavier cells grow faster than lighter ones. The relationship between cell size and growth rate appeared to be linear, and for *B. subtilis* the linear fit extrapolated close to the origin, which is suggestive of a simple exponential growth pattern (**Supplementary Table 1**).

The buoyant mass ranges displayed in **Figure 2** clearly span over twice the lowest values, particularly in the *B. subtilis* data (**Fig. 2a**). Buoyant masses that are more than twice the smallest size in the population could potentially represent multiple cells simultaneously entering the SMR. The larger SMR used to trap the L1210 cells allows for optical microscope access, providing confirmation that the cells are singlets. The devices used for yeast and bacteria are both opaque, but the channel cross-section of the SMR used for yeast greatly reduces the likelihood of trapping clustered

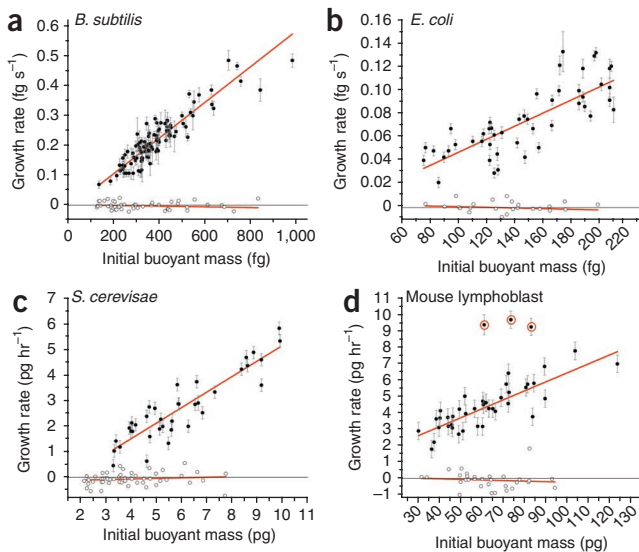


**Figure 2** | Growth rate versus initial buoyant mass. Each data point represents a trapped cell and is plotted on the diagram according to the cell's initial buoyant mass and the measured growth rate during the trapping period. Filled circles indicate normal growing cells and open circles fixed cells. (a) *B. subtilis* (Marburg strain) from nine cultures grown at 37 °C. (b) *E. coli* K12 from 11 cultures grown at 37 °C. (c) *S. cerevisiae* from one culture grown at 30 °C. (d) L1210 mouse lymphoblasts from two cultures grown at 37 °C. Curve fits are weighted linear regressions. The growth rate error bars for the growing cells are  $\pm 1$  s.d. of the growth rate measurements of the fixed cells, except in the cases when the least-squares fitting parameter standard error is greater (owing to particularly short trapping times). See Online Methods and **Supplementary Table 1** for details on culture growth conditions, statistical analysis and experimental errors. **Supplementary Figure 6** shows a small, but nonzero, probability of over- or underdetermining the growth rate. In light of this, the three L1210 cells that had surprisingly high growth rates (circled in red) were not included in the linear regression.

cells. However, for the bacteria, clustering is possible and some of the larger mass values are almost certainly doublets. Note that although our exponential-phase cultures of yeast and mammalian cells were almost entirely composed of single cells when observed under a microscope, both bacterial cultures contained  $\sim 20\%$  non-segregated cells or small clusters (Online Methods). To isolate the single-cell events for bacteria, one could consider only those events that have a buoyant mass less than twice the minimum buoyant mass. It may also, however, be worth recording events above that threshold, as the presence of clustered cells can give additional information of the growth pattern of the cells: a discontinuity of the growth rate at about twice the value of the lowest buoyant masses would be inconsistent with exponential growth of single bacteria (**Supplementary Fig. 5** and **Supplementary Table 2**).

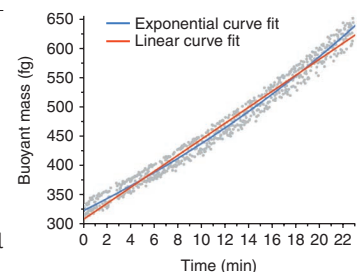
Although the data for all cell types are inconsistent with simple linear growth, measurement errors and cell-to-cell variation could potentially mask growth-rate changes that would identify multiple stages of linear growth during the cell cycle. To evaluate the experimental error of the growth rate determination, we performed similar trapping experiments with fixed cells (Online Methods). As the growth rate of fixed cells is zero, the deviation from this value provides a measure of the experimental error. The cell-to-cell variability in growth rates is generally greater than the error of the method (Online Methods and **Supplementary Fig. 6** for error analysis). That is, the deviations of cells from the fitted curves in **Figure 2** are often not due to experimental error but instead reflect the biological variation in an isogenic population. Cells—even those of the same buoyant mass, but not necessarily at the same cell cycle position—can show different instantaneous growth rates. Previous cell cycle models typically assume that all cells of a given size grow at the same rate<sup>5,13</sup>, and a lack of precision in prior methodologies may have prevented growth-rate variability from being observed until now. For all the cell types measured in **Figure 2**, the single-cell growth rates were consistent with the population doubling time of exponential-phase cultures (**Supplementary Table 3**). This suggests that our system does not alter normal cellular growth, and as we currently have no information on cell cycle position, it is possible that the measured variations reflect cell cycle-dependent changes in growth rate<sup>5,7,9</sup>. A second possibility is that cell growth

is variable in a manner that is independent of cell size and cell cycle position. The source of this variability is unknown, but many transcripts and proteins are subject to stochastic fluctuations in bacteria, yeast and mammalian cells<sup>14</sup>, conceivably influencing growth rate consistency. As previously observed<sup>3,4,15,16</sup>, we have found single-cell growth to be smooth and continuous and do not believe the observed variability occurs abruptly within a cell's lifespan (see discussion below and **Fig. 3**). Further investigations will be required to uncover the true nature of this variability.

We were occasionally able to trap *B. subtilis* for long enough to allow a full cell cycle (**Fig. 3** and **Supplementary Fig. 7**). Optical access was not available to verify the presence of single cells; however, for all three long-duration traps, the initial buoyant mass value was in the lower end of the distribution of buoyant masses for the *B. subtilis* population (**Supplementary Fig. 8**). Therefore, it is likely that only a single cell was present for most of the duration of each long trapping event. When fitting curves to the three long trapping events, we found a simple exponential fit to be a better match than linear or bilinear fits, as verified by four different statistical tests. Results from these long-duration traps support the conclusions of the shorter trapping events with *B. subtilis* (**Fig. 2a**, Online Methods and **Supplementary Table 4** for details of curve fitting). Importantly, analysis of the three long trapping events and the ensemble of shorter 'instantaneous' trapping events yielded a consistent cellular doubling time for *B. subtilis*, further validating the method and findings previously described.

We next implemented a model to describe our experiment and to compare simulated results for linearly and exponentially growing bacterial cells with experimental data, taking into consideration the fact that our system may measure clustered cells. For *B. subtilis*, we found that the trend and the dispersion of the experimental data were well matched by an exponential growth model. For *E. coli*, we were not able to identify the best growth model as a result of the

**Figure 3** | *B. subtilis* cell trapped for a period similar to the cell cycle duration. Data is fitted to linear (red; reduced  $\chi^2 = 0.00257$ ) and exponential (blue; reduced  $\chi^2 = 0.00187$ ) functions. See the **Supplementary Note** and **Supplementary Table 4** for details of the statistical analysis, additional models and model comparison.



high variability of the growth-rate values (**Supplementary Fig. 5**, Online Methods and **Supplementary Table 5** for model details).

Our finding that growth rate is size dependent suggests that these bacterial, yeast and mammalian cell types must actively balance their growth and division. If growth and division rates were not coordinated in cells with size-dependent growth, cell size variation in the population would continually increase<sup>17</sup>, which is not the case. Although molecular mechanisms coordinating growth and division have been described in yeast and bacteria<sup>18</sup>, such mechanisms have not yet been characterized in mammalian cells.

We envision that our dynamic trapping method for measuring cell growth rate can contribute to the study of many cellular processes (for example, growth, the cell cycle, autophagy, apoptosis, cell differentiation) as well as cellular models of disease states. Future versions of this system will provide even more experimental power. It will be possible to simultaneously measure the buoyant mass, volume and density of a trapped, growing cell by periodically modulating the solution density within the SMR. In addition, optical access to the trapped cell will allow dynamic cellular and molecular information to be garnered from fluorescent reporters and then correlated in real-time with cell growth.

## METHODS

Methods and any associated references are available in the online version of the paper at <http://www.nature.com/naturemethods/>.

*Note: Supplementary information is available on the Nature Methods website.*

## ACKNOWLEDGMENTS

Funding was provided by EUREKA (R01GM085457) and a Center for Cell Decision Process Grant (P50GM68762) from the US National Institute of Health and by an Institute for Collaborative Biotechnologies Grant (DAAD1903D0004) from the US Army Research Office. M.G. acknowledges support from the Natural Sciences and Engineering Research Council of Canada. F.F.D. acknowledges support from Fundação para a Ciência e a Tecnologia, Portugal, through a graduate fellowship (SFRH/BD/47736/2008).

Devices were fabricated at the Massachusetts Institute of Technology's Microsystems Technology Laboratory and at Innovative Micro Technologies.

## AUTHOR CONTRIBUTIONS

M.G. developed the trapping method, F.F.D. developed the model, M.G. and F.F.D. conducted experiments on bacteria, W.H.G. and A.K.B. adapted the method and conducted experiments on yeast, and S.S. adapted the method and conducted experiments on mouse lymphoblasts. K.P. fabricated the devices used for experiments on mouse lymphoblasts. All authors contributed to designing of the experiments and writing of the manuscript.

## COMPETING FINANCIAL INTERESTS

The authors declare competing financial interests: details accompany the full-text HTML version of the paper at <http://www.nature.com/naturemethods/>.

Published online at <http://www.nature.com/naturemethods/>.

Reprints and permissions information is available online at <http://npg.nature.com/reprintsandpermissions/>.

1. Kubitschek, H.E. *J. Bacteriol.* **168**, 613–618 (1986).
2. Cullum, J. & Vicente, M. *J. Bacteriol.* **134**, 330–337 (1978).
3. Reshes, G., Vanounou, S., Fishov, I. & Feingold, M. *Biophys. J.* **94**, 251–264 (2008).
4. Schaechter, M., Williamson, J.P., Hood, J.R. Jr. & Kochal, J. *Gen. Microbiol.* **29**, 421–434 (1962).
5. Di Talia, S., Skotheim, J.M., Bean, J.M., Siggia, E.D. & Cross, F.R. *Nature* **448**, 947–951 (2007).
6. Elliott, S.G. & McLaughlin, C.S. *Proc. Natl. Acad. Sci. USA* **75**, 4384–4388 (1978).
7. Goranov, A.I. *et al. Genes Dev.* **23**, 1408–1422 (2009).
8. Conlon, I. & Raff, M. *J. Biol.* **2**, 7 (2003).
9. Tzur, A., Kafri, R., LeBleu, V.S., Lahav, G. & Kirschner, M.W. *Science* **325**, 167–171 (2009).
10. Efe, J.A., Botelho, R.J. & Emr, S.D. *Curr. Opin. Cell Biol.* **17**, 402–408 (2005).
11. Popescu, G. *et al. Am. J. Physiol. Cell Physiol.* **295**, C538–C544 (2008).
12. Burg, T.P. *et al. Nature* **446**, 1066–1069 (2007).
13. Chen, K.C. *et al. Mol. Biol. Cell* **15**, 3841–3862 (2004).
14. Raj, A. & van Oudenaarden, A. *Cell* **135**, 216–226 (2008).
15. Prescott, D.M. *Exp. Cell Res.* **9**, 328–337 (1955).
16. Reshes, G., Vanounou, S., Fishov, I. & Feingold, M. *Phys. Biol.* **5**, 46001 (2008).
17. Tyson, J.J. & Hannsgen, K.B. *J. Math. Biol.* **22**, 61–68 (1985).
18. Jorgensen, P. & Tyers, M. *Curr. Biol.* **14**, R1014–R1027 (2004).

## ONLINE METHODS

**Cell culture conditions.** *B. subtilis* (ATCC no. 6051) and *E. coli* (ATCC no. 23725) were grown in Luria-Bertani (Miller) broth (Sigma no. L2542) supplemented with 0.5% BSA (Sigma no. A3059) overnight at 37 °C or 23 °C and then diluted 1:100 in the same heated medium, 1–2 h before the measurement. Samples were introduced into the device at concentrations ranging between  $1 \times 10^6$  and  $1 \times 10^7$  ml<sup>-1</sup>. Doubling times for bacteria were determined by turbidity measurements at 560 nm: *E. coli*:  $26 \pm 3$  min ( $n = 10$ ) at 37 °C and  $65 \pm 2$  min ( $n = 3$ ) at 23 °C; *B. subtilis*:  $20 \pm 1$  min ( $n = 5$ ). *S. cerevisiae* were grown overnight at 23 °C in YEP (yeast extract plus peptone) medium containing 2% glucose and 1 mg ml<sup>-1</sup> adenine. The overnight culture was then diluted 1:250 in the same medium and maintained at 30 °C during measurement. A doubling time of  $1.60 \pm 0.04$  h at 30 °C ( $n = 6$ ) was determined by optical absorbance at 600 nm. Yeast were introduced into the device at concentrations ranging between  $1 \times 10^5$  and  $1 \times 10^6$  ml<sup>-1</sup>. L1210 mouse lymphocytes were grown in L-15 medium (Invitrogen no. 21083027) supplemented with 10% FBS (Invitrogen no. 16000-044), 0.4% glucose (Sigma no. G8769) and 1% penicillin/streptomycin mix (Cellgro no. MT-30-002-CI) at 37 °C. Doubling time was 12 h at exponential growth phase and was determined by cell concentration measured with a Coulter counter. Samples were introduced into the device at concentrations ranging between  $5 \times 10^4$  and  $2 \times 10^5$  ml<sup>-1</sup>.

**Experimental setup and measurement conditions.** Details of the fabrication of the SMR, instrumentation for data acquisition and software for data analysis have been previously reported<sup>12</sup>.

Precision pressure regulators (electronically controlled Proportion Air QPV1 and manually controlled Omega PRG101-25) were used to control sample flow within the SMR. These regulators provided the necessary stability to precisely control the position of the target cell within the 15- and 191-pI internal volumes of the  $3 \times 8$ - $\mu$ m and  $15 \times 20$ - $\mu$ m suspended microchannels. Glass vials with open-top caps and Teflon-lined septa were used to contain the samples and collect sample waste. Ultra-high-purity nitrogen was used to pressurize the contents of the vials for sample introduction into the microfluidic device and for fluidic flow control.

During an experiment, a dilute sample containing the target cells ( $\sim 10^5$ – $10^7$  ml<sup>-1</sup>) is introduced into the two bypass channels (cross-sectional size  $30 \times 80$   $\mu$ m) on each side of the suspended microchannel (cross-sectional size  $3 \times 8$  microns for bacteria and  $15 \times 20$   $\mu$ m for L1210 cells). The pressures at all four ports are equalized to limit sample flow in the bypass channels and through the suspended microchannel. A computer-controllable pressure regulator is then used at the outlet port of one of the bypass channels to apply a slight pressure differential across the suspended microchannel promoting a small flow through the SMR. Custom-made feedback software, implemented with National Instruments LabVIEW, then waits for a single cell to enter the SMR. Once a mass measurement is acquired, the software automatically adjusts the pressure to reverse the flow direction within the suspended microchannel. The algorithm also maintains a constant flow rate ( $\sim 20$  pl s<sup>-1</sup>) by monitoring the cell transit times (duration of the transient frequency shifts) during each passage. The feedback software compensates for any pressure drifts that occur over extended periods of time.

For yeast measurements, a slightly different experimental setup and  $8 \times 8$ - $\mu$ m suspended microchannels were used. A stirred cell culture at atmospheric pressure is connected via capillary tubing to the inputs of the SMR bypass channels. The outputs of the bypass channels are connected via tubing to two waste vials. Two solenoid valves and a vacuum regulator (SMC no. ITV2090) are used to selectively depressurize the contents of one waste vial while venting the other vial to the atmosphere. Switching the solenoid valves alternates which vial is depressurized and reverses the direction of fluid flow in the SMR. By switching the solenoid valves immediately after a cell passes through the SMR, the cell can be routed back and forth through the SMR several times per second, measuring the buoyant mass of the cell with every pass.

Fixed cells were incubated for 1 h in a solution of 3.7% formaldehyde and 2% glutaraldehyde in 100 mM PBS (Cellgro), after being twice pelleted (3 min at 3,000g) and resuspended in PBS to wash away the growth medium.

The SMR microchannel and fluidic system are sterilized with piranha solution (1:3 mixture of hydrogen peroxide and sulfuric acid) and thoroughly rinsed for  $\sim 1$  h with deionized water and growth medium before measurements. Polystyrene size standard (National Institute of Standards and Technology) particles (diameter 1.51  $\mu$ m, Bangs Laboratories NT16N, for the suspended microchannel of  $3 \times 8$   $\mu$ m and  $8 \times 8$   $\mu$ m; diameter 8.62  $\mu$ m, Bangs Laboratories NT25N, for the  $15 \times 20$   $\mu$ m) dispersed in water are used to calibrate the device for mass. The device is installed in a metal clamp connected to a water circulator (Thermo NESLAB RTE7) that maintains the SMR at constant temperature, as measured using a surface-mounted thermistor connected directly onto the device. The temperature can be adjusted quickly using a thermoelectric module and a temperature controller (Wavelength Electronics Inc.). The pressurized sample vials are also temperature controlled. During an experiment, care is taken to maintain the sample temperature (both before and after cells enter the SMR) at the desired temperature.

For population characterization, the system can be run in a flowthrough mode in which cells are not trapped but measured only once. Buoyant mass distributions of hundreds of single measurements allow the characterization of the culture and, if desired, the selection of a cell on the basis of its buoyant mass<sup>19</sup>.

**Experimental errors.** The growth-rate measurement errors were determined as the s.d. of the growth rate measurements of the fixed cells, except in the cases when the least-squares fitting parameter standard error is greater (owing to particularly short trapping times; description of curve fitting in **Supplementary Note**). **Supplementary Figure 6** characterizes the distribution of growth rate determination errors. The initial buoyant mass errors were determined as the standard error of the  $y$ -intercept fitting parameter (refer to **Supplementary Note**), but their values are too low to be visible in the plots. For the different cell types, they range approximately as follows: *B. subtilis*, 0.7–5.2 fg (0.3–0.7%); *E. coli*, 0.3–0.9 fg (0.3–0.4%); *S. cerevisiae*, 4–8 fg (0.05–0.16%); L1210, 18–96 fg (0.05–0.13%).

**Simulation and growth models.** We implemented a model to simulate the bacterial growth experiments and to extract information concerning the kinetics of cell growth. The simulation models two different populations of growing cells according to

two different growth models, an exponential and a linear one, and measures their growth rates at a random point in the cell cycle. The simulation requires that all cells have specified starting buoyant mass and growth rate (both with certain Gaussian variabilities) and are allowed to grow for three generations. To simulate our experiment, each cell's buoyant mass and growth rate are determined at a random point in its cell cycle. These values are then blurred by simulated experimental errors attributed to the method itself: the uncertainty in the determination of the growth rate (which is inversely proportional to the duration of the trap) and the uncertainty in the cell buoyant mass (which is related to the mass resolution of the device and the trapping duration). The errors are assumed to have Gaussian distributions.

The mathematical expressions for the two growth models are, for linear growth:

$$\begin{cases} m(0) = m_0 \\ m(t+1) = m(t) + b_L \end{cases}$$

and for the exponential growth model:

$$\begin{cases} m(0) = m_0 \\ m(t+1) = m(t) \cdot b_E \end{cases}$$

where  $m_0$  is the starting buoyant mass,  $m(t)$  the time-dependent buoyant mass,  $b_L$  the arithmetic progression difference and  $b_E$  the geometric progression ratio. Cell division is assumed to be symmetrical and occurs at a defined  $t_D$  after which cells may or may not segregate according to a probability  $p_D$  of segregation. For the linear growth model,  $b_L$  is doubled if a cell does not segregate. In the case that a cell does segregate, one of the daughter cells is discarded.

Simulations of the linear and exponential growth models for *B. subtilis* and *E. coli* are shown in **Supplementary Figure 5**. The parameters used in the simulations are listed in **Supplementary Table 5**.

Whenever possible, the parameters were derived from experimental data or literature reports. The errors in the determination of the growth rate and the determination of the cell buoyant

mass are derived from the errors obtained from the fixed cells' experimental data (see section on Experimental errors above); the initial peak height are averages from the individual cell buoyant mass data ( $n = 100$  for *B. subtilis* and  $n = 48$  for *E. coli*). The probability of segregation is the ratio of single cells versus non-single cells and was estimated by counting single cells and clustered/nonsegregated cells by optical microscopy ( $n > 1,000$ ). The doubling time is an average of culture doubling times determined by turbidity measurements ( $n = 5$  for *B. subtilis* and  $n = 10$  for *E. coli*). The cell-growth parameters  $b_L$  and  $b_E$  are calculated as the values needed to double the initial mass size during the doubling time. For the exponential case, this parameter is a time constant independent of the starting buoyant mass. The cell starting buoyant mass (that is, the weight of cell at the beginning of the simulation and immediately after division) is a fit parameter because of the lack of experimental values. For both bacterial strains ~10% of the cells have buoyant masses below this value. The growth parameter errors are also fit parameters, and we report the minimum apparent values that fit the dispersion of the experimental data. For *E. coli*, cell length variability at birth of ~35% and coefficients of variability for linear growth rates of cell length >28% are reported in the literature<sup>16</sup>; the s.d. values used for the initial cell size distribution and growth parameters are consistent with such reporting. The model is robust in that substantial changes in the fit parameters ( $\pm 20\%$ ) do not significantly alter the results. Buoyant mass distributions can be obtained from the simulated data (**Supplementary Fig. 8**).

A bilinear growth model, in which the rate change point might occur elsewhere than at division, was not considered in our simulations, as one would have to introduce other parameters in the model without any experimental cue to support them, such as septum formation. Yet, for the *B. subtilis*, such a model would again predict a discontinuity in the growth rate which we did not observe in the experimental data.

19. Godin, M., Bryan, A.K., Burg, T.P., Babcock, K. & Manalis, S.R. *Appl. Phys. Lett.* **91**, 123121 (2007).



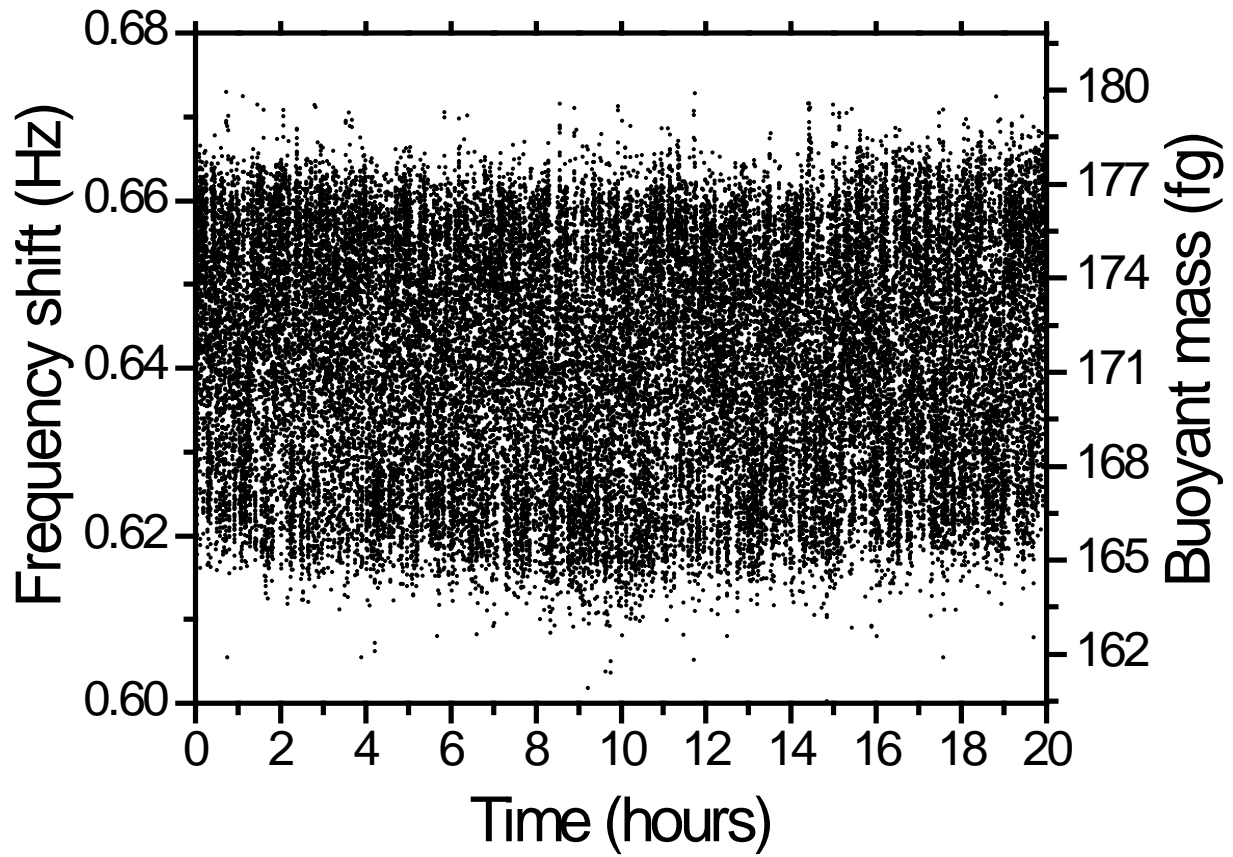
## Using buoyant mass to measure the growth of single cells

Michel Godin, Francisco Feijó Delgado, Sungmin Son, William H Grover, Andrea K Bryan, Amit Tzur, Paul Jorgensen, Kris Payer, Alan D Grossman, Marc W Kirschner & Scott R Manalis

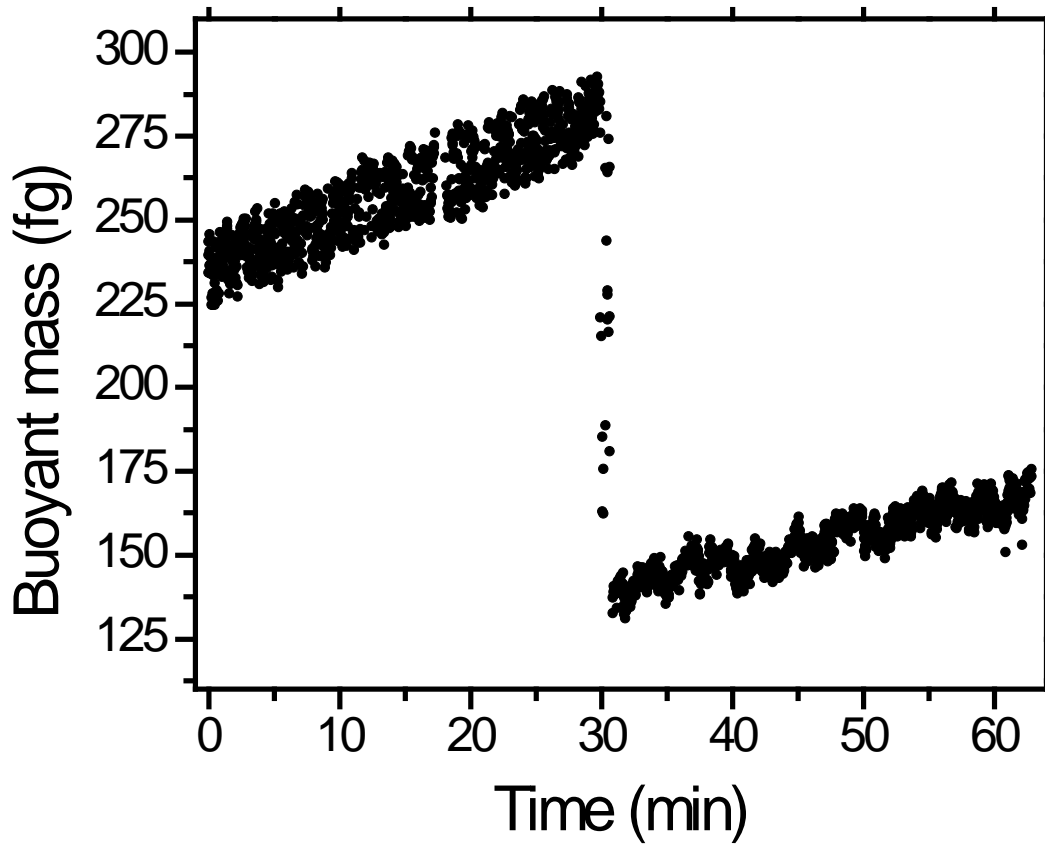
Supplementary figures and text:

<b>Supplementary Figure 1</b>	Trapping of a polystyrene particle.
<b>Supplementary Figure 2</b>	Cellular segregation of <i>E. coli</i> cells growing at 23°C.
<b>Supplementary Figure 3</b>	Addition of the poison sodium azide to a culture of <i>S. cerevisiae</i> inhibits cell growth, demonstrating that the sequential increase in buoyant mass is due to cell growth..
<b>Supplementary Figure 4</b>	Growth rate versus initial buoyant mass of <i>E. coli</i> grown at different temperatures.
<b>Supplementary Figure 5</b>	Output of the model for the trapping data.
<b>Supplementary Figure 6</b>	Histogram of normalized growth rates of the fixed cells.
<b>Supplementary Figure 7</b>	Additional <i>B. subtilis</i> long trapping events.
<b>Supplementary Figure 8</b>	Experimental and simulated buoyant mass distributions.
<b>Supplementary Table 1</b>	Curve fit parameters of data presented in Figure 2 and in Supplementary Figure 4.
<b>Supplementary Table 2</b>	Fit parameters and model selection criteria values for linear and stepwise function curve fits to bacterial trapping data.
<b>Supplementary Table 3</b>	Culture doubling times obtained by standard techniques and estimated from SMR data.
<b>Supplementary Table 4</b>	Fit parameters and model selection criteria values for linear, bilinear and exponential curve fits to long trapping events of <i>B. subtilis</i> .
<b>Supplementary Table 5</b>	Simulation parameters used to generate Supplementary Figure 5.
<b>Supplementary Note</b>	Data analysis, curve fitting and model selection criteria

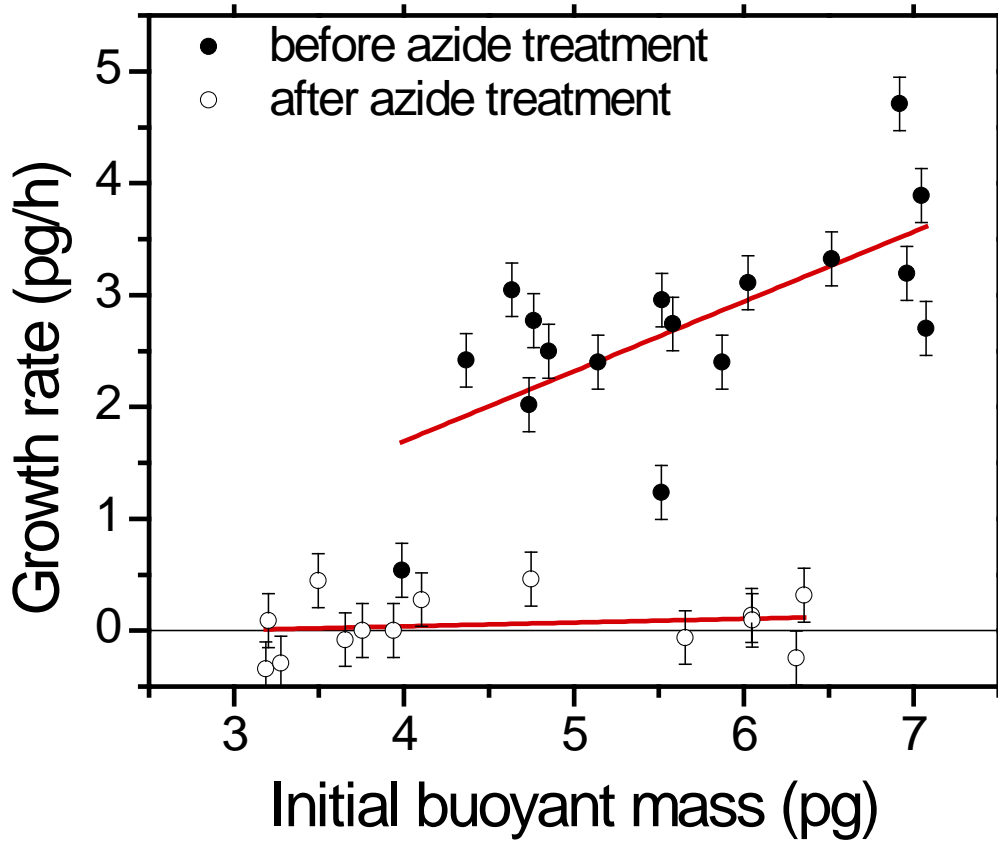
## Supplementary Figures



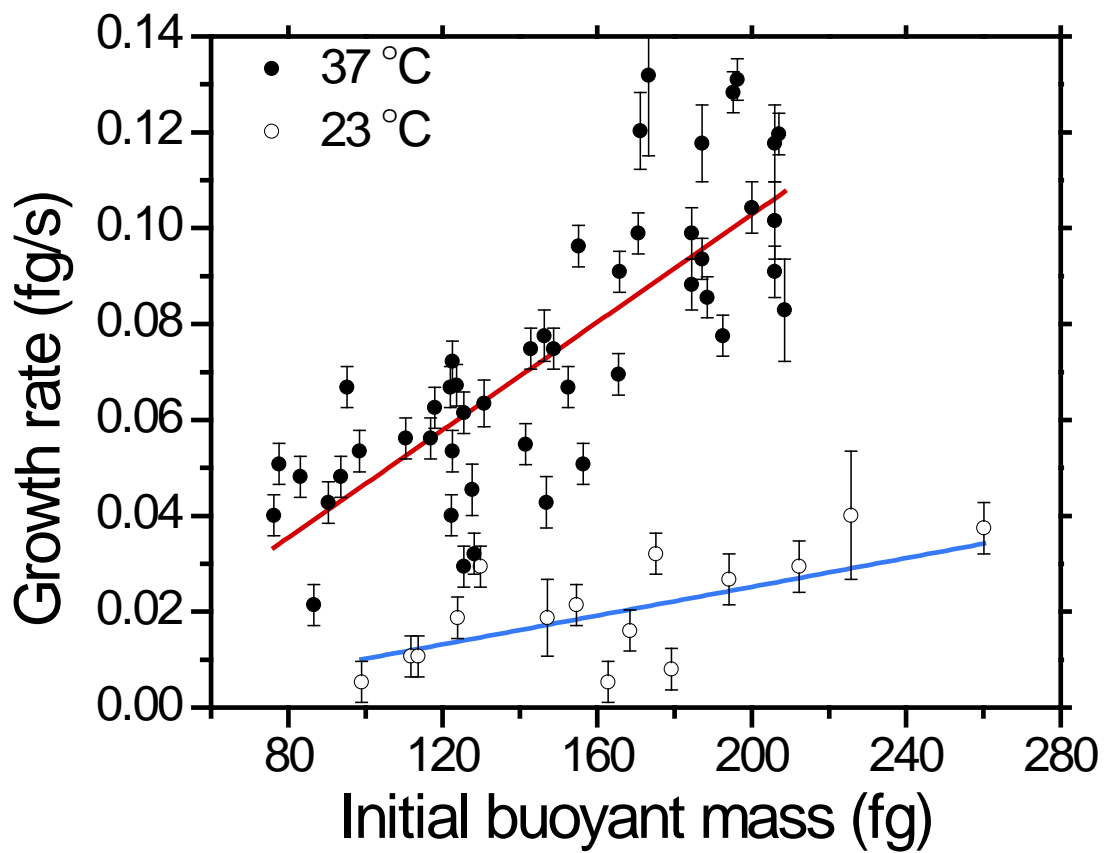
**Supplementary Figure 1** – Trapping of a polystyrene particle. The data show more than 32,000 consecutive buoyant mass measurements of a single 1.90 $\mu\text{m}$  diameter polystyrene particle.



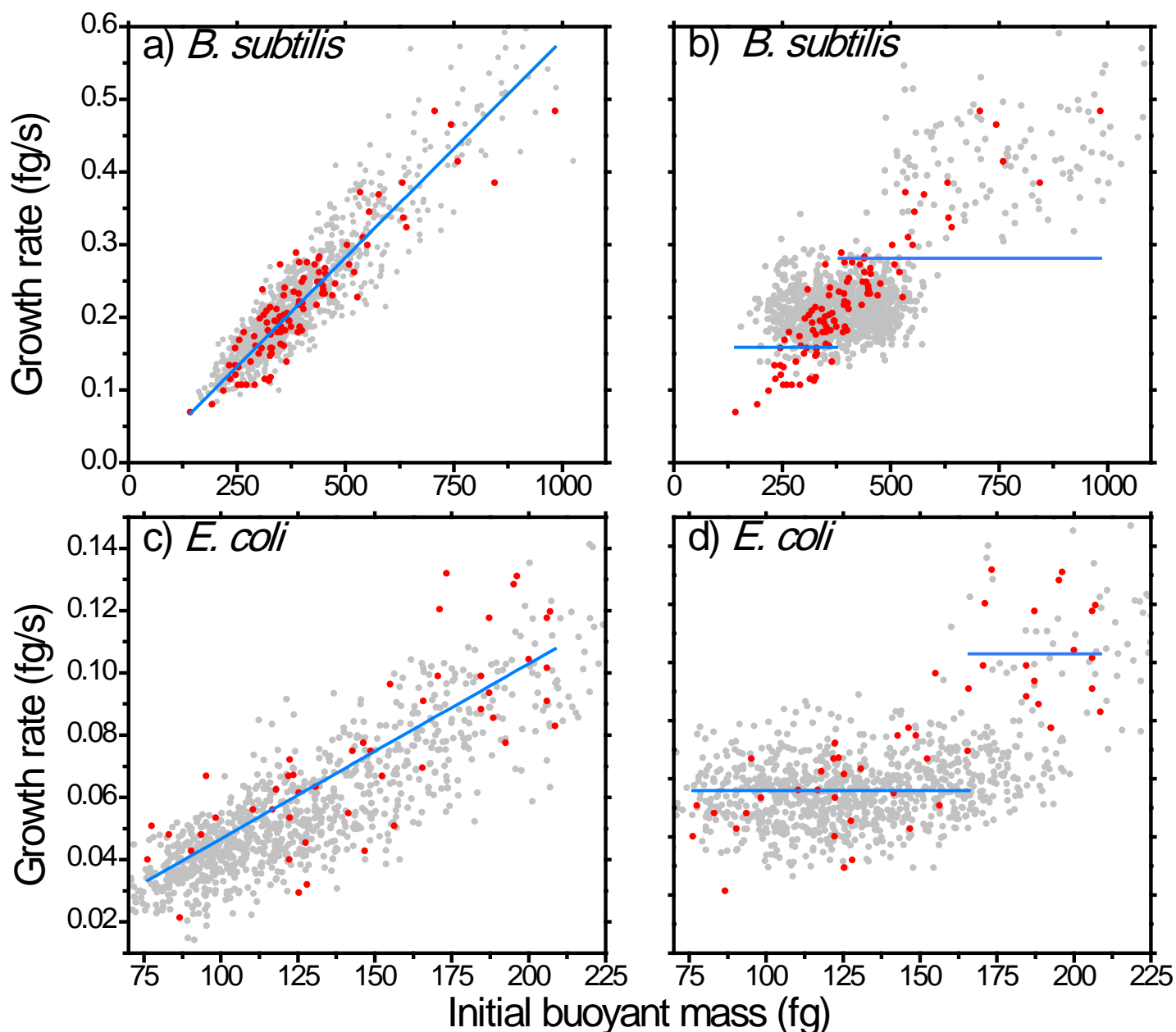
**Supplementary Figure 2** – Cellular segregation of *E. coli* cells growing at 23°C. A growing cell, or possibly a cluster of two cells if division had occurred previously, segregates at  $t = 30$  min. A brief period occurs during which both cells remain trapped and the trap is unstable as the feedback system can only track one cell. In this case one of the daughter cells escapes the trap while the other remains inside the SMR. The buoyant mass ratio at the segregation time is  $2.1 \pm 0.2$  and the growth rate ratio is  $1.67 \pm 0.07$ .



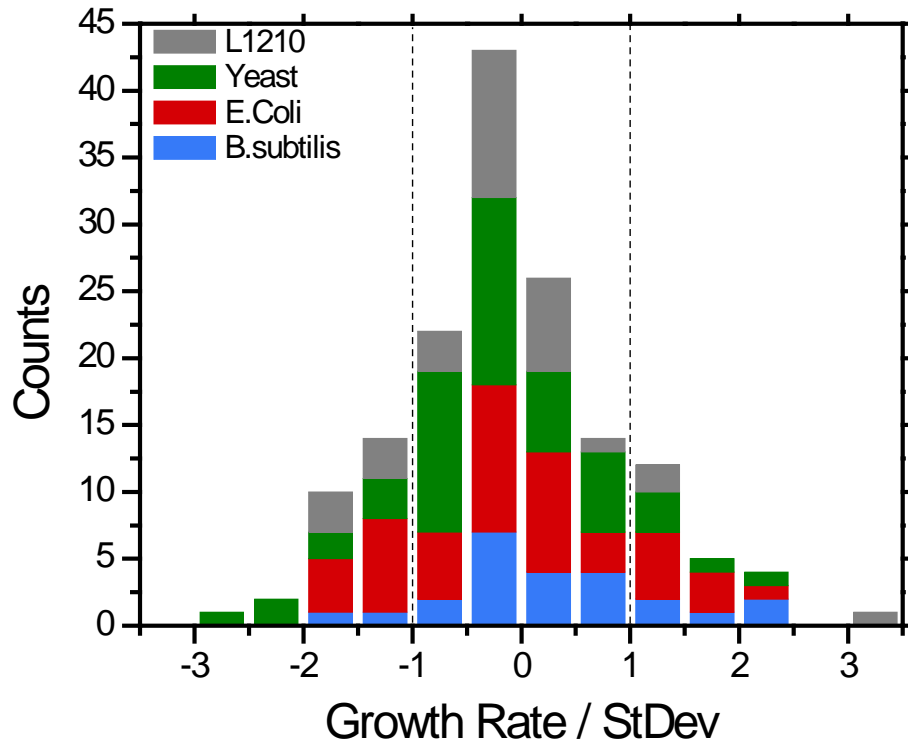
**Supplementary Figure 3** - Addition of the poison sodium azide to a culture of *S. cerevisiae* inhibits cell growth, demonstrating that the sequential increase in buoyant mass is due to cell growth.



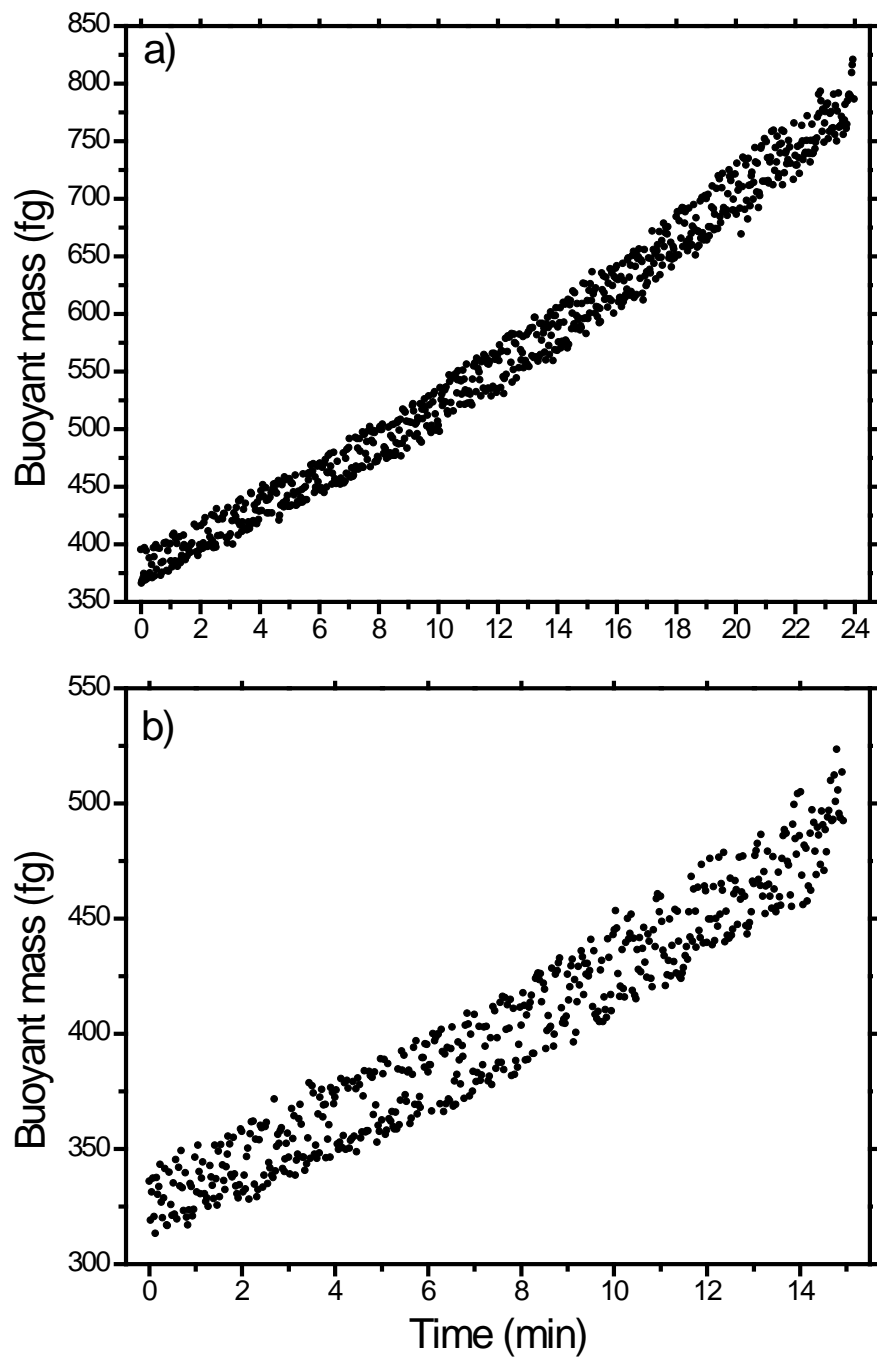
**Supplementary Figure 4** - Growth rate *versus* initial buoyant mass at different temperatures. *E. coli* cells were grown at 37 °C (filled circles) and 23°C (open circles). Fit parameters are reported in **Supplementary Table 1**.



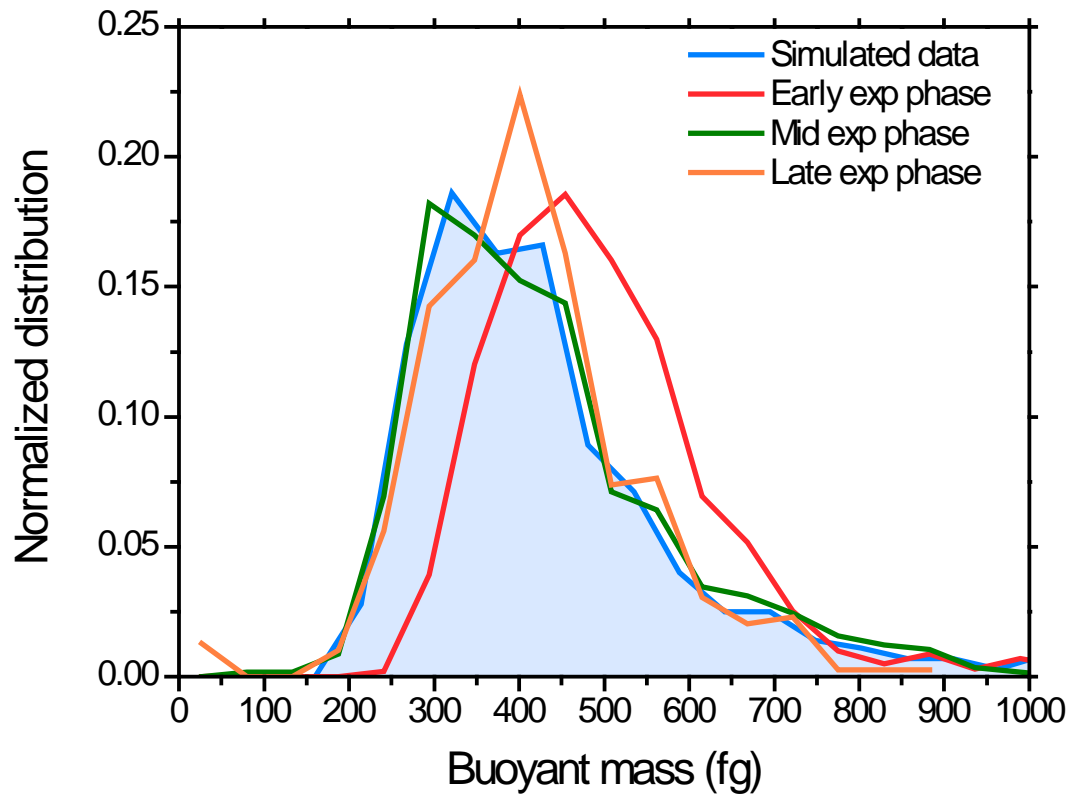
**Supplementary Figure 5** – Models for cell trapping data. The plots show the overlap between experimental data (red) obtained for **a), b)** *Bacillus subtilis* and **c), d)** *E. coli* and simulated data (grey) obtained using an exponential growth law **a), c)** and a linear growth law **b), d)**. Blue lines are weighted curve fits of the experimental data to a linear curve **a), c)** and a piecewise constant function **b), d)**. Error bars are not presented here for clarity, but are shown in **Figure 2**. Details of the modeling and curve fitting are in the **Supplementary Note**; curve fit parameters and model selection criteria results are reported in **Supplementary Table 2**. The initial cell buoyant mass represents the buoyant mass value of a cell when it is introduced into the trap. For the simulation data, these values correspond to the cell cycle time point at which the cells were randomly selected to be measured. For *B. subtilis* **a), b)**, the results are clearly better matched by the exponential model, which describes both the trend and the dispersion of mass measurements. The linear model outputs two distinguishable populations (single cells and doublets), unlike the exponential model where the two populations overlap. Such discontinuity in the growth rate is not observed in the experimental results. For *E. coli* **c), d)**, however, the match is not as clear and therefore the modelling does not allow for a definitive distinction. All the model selection criteria for the experimental data curve fits (blue) favor the linear fit for both organisms, yielding parameters similar to the ones used in the simulation. Integrating  $\frac{dm}{dt} = a \cdot m + b$  yields  $m(t) = m_0 e^{at} - \frac{b}{a}$  indicating that the above curve fits both favor the exponential growth model. For the *B. subtilis* case the distinction is greater and the fit parameter  $b = -0.0179 \pm 0.0109$ , consistent with a line intercepting the origin, suggests a simple exponential growth pattern.



**Supplementary Figure 6** – Histogram of the growth rates of the fixed (non-growing) cells normalized by the standard deviation of each cell type (*B. subtilis*: 0.012 fg/s, *E. coli*: 0.004 fg/s, *S. cerevisiae*: 0.53pg/h, **L1210**: 0.24pg/h) in order to compare across systems. Total cell count is 154. The distribution characterizes our growth rate measurement error: approximately 68% of the cells have growth rates between  $\pm$  one standard deviation, denoted by the dashed lines, which represent the size of the error bars.



**Supplementary Figure 7** – Additional *B. subtilis* long trapping events.



**Supplementary Figure 8** - Experimental and simulated buoyant mass distributions. The plots show normalized (area under the curve) buoyant mass distribution for several exponentially growing cultures of *B. subtilis* that were obtained by running the SMR in a flow-through mode, where no trapping occurs ( $n = 1024, 577$  and  $393$  for early, mid and late cultures). The simulated distribution (blue with shaded area under the curve) is extracted from modeled data presented in **Supplementary Figure 5** ( $n = 1000$ ) and fits well to experimental results. This result doesn't show a distinction between the linear and exponential models, as expected, but does allow for comparison between model predictions and experimental data.

## Supplementary Tables

**Supplementary Table 1** – Fit parameters for the linear regressions presented in **Figure 2** and **Supplementary Figure 4**.

Cells	n	Parameters	R <sup>2</sup>	χ <sup>2</sup>
<i>B. subtilis</i>	100	$a = 6.00 \times 10^{-4} \pm 2.6 \times 10^{-6} \text{ s}^{-1}$ , $b = -0.0179 \pm 0.0109 \text{ fg/s}$	0.8548	3.857
<i>E. coli</i>	48	$a = 5.62 \times 10^{-4} \pm 6.4 \times 10^{-5} \text{ s}^{-1}$ , $b = -0.0095 \pm 0.0098 \text{ fg/s}$	0.6469	11.814
<i>E. coli</i> (23°C)	15	$a = 1.50 \times 10^{-4} \pm 5.0 \times 10^{-5} \text{ s}^{-1}$ , $b = -0.0048 \pm 0.0085 \text{ fg/s}$	0.3032	3.497
<i>S. cerevisiae</i>	36	$a = 0.608 \pm 0.049 \text{ hr}^{-1}$ , $b = -0.964 \pm 0.306 \text{ pg/hr}$	0.8092	5.557
Mouse lymphoblasts	39	$a = 0.055 \pm 0.006 \text{ hr}^{-1}$ , $b = 0.901 \pm 0.388 \text{ pg/hr}$	0.6783	1.969

Refer to the Online Methods for the definition of the fit parameters, R<sup>2</sup> and χ<sup>2</sup>

**Supplementary Table 2** – Fit parameters and model selection criteria values for linear and stepwise function curve fits to bacterial trapping data. Fit curves are superimposed to data presented in **Supplementary Figure 5**.

	Model	n	Parameters	R <sup>2</sup>	χ <sup>2</sup>	AIC	SBIC
<i>B. subtilis</i>	Linear	100	$a = 6.00 \times 10^{-4} \pm 2.6 \times 10^{-6} \text{ s}^{-1}$ , $b = -0.0179 \pm 0.0109 \text{ fg/s}$	<b>0.8548</b>	<b>3.857</b>	<b>137.08</b>	<b>142.17</b>
	Stepwise		$b_1 = 0.159 \pm 0.027 \text{ fg/s}$ , $b_2 = 0.281 \pm 0.010 \text{ fg/s}$ , $m_c = 378 \text{ fg}$	0.5217	12.701	257.38	264.94
<i>E. coli</i>	Linear	48	$a = 5.62 \times 10^{-4} \pm 6.4 \times 10^{-5} \text{ s}^{-1}$ , $b = -0.0095 \pm 0.0098 \text{ fg/s}$	<b>0.6469</b>	<b>11.814</b>	<b>120.75</b>	<b>124.22</b>
	Stepwise		$b_1 = 0.056 \pm 0.019 \text{ fg/s}$ , $b_2 = 0.103 \pm 0.005 \text{ fg/s}$ , $m_c = 166 \text{ fg}$	0.6051	120.80	233.56	238.65

Refer to the Supplementary Note for the definition of the fit parameters, R<sup>2</sup>, χ<sup>2</sup>, AIC and SBIC

**Supplementary Table 3** – Culture doubling times obtained by standard techniques and estimated from SMR data.

Cells	Doubling time from SMR data	Culture doubling time
<i>B. subtilis</i>	19.3min	20±1 min
<i>E. coli</i>	20.6 min	26±3 min
<i>E. coli</i> (23°C)	77 min	65±2 min
<i>S. cerevisiae</i>	1.1 hr*	1.60±0.04 hr
Mouse lymphoblasts	12.6 hr	12 hr

See **Online Methods** for details on the measurement of culture doubling times. Cellular doubling times are estimated with the assumption of simple exponential growth. The doubling time is then  $t_d = \ln 2 / a$ , where  $a$  is the respective slope of the linear fits in **Figure 2** and **Supplementary Figure 4** (listed in **Supplementary Table 1**). \*Several factors complicate the calculation of a doubling time from single-cell growth rate data for yeast: mother and daughter cells have unequal sizes at cell division, mothers and daughters have different doubling times, and daughters more than double their mass during their first cell cycle<sup>S3 S4</sup>. Without information about each cell's age and position within the cell cycle, the simple exponential fit of the experimental data represents only an approximation of the overall growth rate, and the resulting calculated doubling time (1.1 h) has only fair agreement with the actual bulk culture doubling time (1.6 h).

**Supplementary Table 4** – Fit parameters and model selection criteria values for linear, bilinear and exponential curve fits to long trapping events of *B. subtilis*. Data are presented in **Figure 3** and **Supplementary Figure 7**.

Refer to the Supplementary Note for the definition of the fit parameters,  $R^2$ ,  $\chi^2$ , AIC and SBIC

**Curve 1 (Fig. 3)**

Duration: 23.3 mins  
Data points: 764  
Initial buoyant mass: 313.3 fg  
Final buoyant mass: 672.7 fg

Model	$R^2$	$\chi^2$	AIC	SBIC
Linear	0.9785	183.47	3984.01	3993.26
Exponential	<b>0.9842</b>	<b>134.72</b>	<b>3748.07</b>	<b>3757.33</b>
Bilinear	0.9841	135.33	3945.58	3964.08

Fit parameters:

- Linear:  $a = 0.228 \pm 0.001$  fg/s;  $b = 308.23 \pm 0.99$  fg
- Exponential:  $A_0 = 325.41 \pm 0.70$  fg;  $a = 4.91 \times 10^{-4} \pm 2.3 \times 10^{-6}$  s<sup>-1</sup>
- Bilinear:  $a_1 = 0.199 \pm 0.002$  fg/s;  $b_1 = 318.90 \pm 1.00$ ;  $a_2 = 0.269 \pm 0.004$  fg/s;  $b_2 = 264.40 \pm 5.03$  fg;  $t_c = 779$ s

**Curve 2 (Supplementary Fig. 7a)**

Duration: 24.0 mins  
Data points: 814  
Initial buoyant mass: 395.1 fg  
Final buoyant mass: 786.6 fg

Model	$R^2$	$\chi^2$	AIC	SBIC
Linear	0.9810	263.70	4539.90	4549.29
Exponential	<b>0.9862</b>	<b>191.39</b>	<b>4279.03</b>	<b>4288.42</b>
Bilinear	0.9862	192.09	4509.52	4528.28

Fit parameters:

- Linear:  $a = 0.285 \pm 0.001$  fg/s;  $b = 358.01 \pm 1.16$  fg
- Exponential:  $A_0 = 382.31 \pm 0.80$  fg;  $a = 5.077 \times 10^{-4} \pm 2.2 \times 10^{-6}$  s<sup>-1</sup>
- Bilinear:  $a_1 = 0.229 \pm 0.004$  fg/s;  $b_1 = 376.28 \pm 1.26$ ;  $a_2 = 0.316 \pm 0.003$  fg/s;  $b_2 = 325.69 \pm 3.01$ ;  $t_c = 585$ s

**Curve 3 (Supplementary Fig. 7b)**

Duration: 14.9 mins  
Data points: 546  
Initial buoyant mass: 336.0 fg  
Final buoyant mass: 492.3 fg

Model	$R^2$	$\chi^2$	AIC	SBIC
Linear	0.9329	164.92	2789.60	2798.18
Exponential	<b>0.9380</b>	<b>152.35</b>	<b>2746.33</b>	<b>2754.91</b>
Bilinear	0.9378	152.96	2768.45	2785.59

Fit parameters:

- Linear:  $a = 0.185 \pm 0.002$  fg/s;  $b = 318.37 \pm 1.09$  fg
- Exponential:  $A_0 = 323.67 \pm 0.94$  fg;  $a = 4.64 \times 10^{-4} \pm 5.13 \times 10^{-6}$  s<sup>-1</sup>
- Bilinear:  $a_1 = 0.160 \pm 0.007$  fg/s;  $b_1 = 324.24 \pm 1.48$  fg;  $a_2 = 0.211 \pm 0.005$  fg/s;  $b_2 = 301.27 \pm 3.25$  fg;  $t_c = 449$ s

For the three curves, the exponential model scores as the one that better describes the experimental data. Since the SMR used for the bacterial measurements is opaque, one cannot visually inspect the cell in order to have cell cycle cues. Therefore, one cannot determine that these trapping curves represent the entirety of a cell cycle or even that the initial buoyant mass is of a newly born cell. For the two first curves, which span a duration consistent with the culture doubling time, the buoyant mass essentially doubles. In addition, the initial buoyant masses are located on the lower end of the buoyant mass spectrum. Therefore it is likely that single cells were being trapped for the majority of the trapping events.

**Supplementary Table 5** – Simulation parameters used to generate **Supplementary Figure 5**.

PARAMETER	VALUE ( <i>B. subtilis</i> )	VALUE ( <i>E. coli</i> )
cell growth parameter exponential [ $b_E$ ]	$\mu = \ln 2 \div t_D = 5.69 \times 10^{-4}$ $\sigma = 10\% \cdot \mu$	$\mu = \ln 2 \div t_D = 4.43 \times 10^{-4}$ $\sigma = 18\% \cdot \mu$
linear [ $b_L$ ]	$\mu = m_0 \div t_D = 0.171$ $\sigma = 10\% \cdot \mu$	$\mu = m_0 \div t_D = 0.055$ $\sigma = 18\% \cdot \mu$
cell starting buoyant mass (at t=0) [ $m_0$ ]	$\mu = 255$ fg $\sigma = 15\% \cdot \mu$	$\mu = 86$ fg $\sigma = 16\% \cdot \mu$
doubling time [ $t_D$ ]	20.3 min	26.1 min
probability of segregation [ $\rho_D$ ]	85%	82%
error in determination of the growth rate	$\mu = 0$ $\sigma = 11\%$	$\mu = 0$ $\sigma = 7.7\%$
error in determination of the cell size	$\mu = 0$ $\sigma = 0.7\%$	$\mu = 0$ $\sigma = 0.4\%$
number of cells	1000	1000

## Supplementary Note

**Data analysis and curve fitting.** Curve fittings to linear models were performed in MATLAB by calculating weighted linear least square fits. The fits to the data presented in **Figure 2** and **Supplementary Figure 5** had the form  $\frac{dm}{dt} = a \cdot m + b$ , where the  $m$  is the buoyant mass, and experimental errors ( $\varepsilon_i$ ) used as fitting weights ( $1/\varepsilon_i^2$ ). Fit parameters for the linear regressions and their standard errors are presented in **Supplementary Tables 1,2**. In addition, bacterial experimental data were fitted to a piecewise function (**Supplementary Fig. 5**) of the form  $\frac{dm}{dt} = b_1$  for  $m < m_C$ ;  $\frac{dm}{dt} = b_2$  for  $m > m_C$ , where  $m_C$  is the mass threshold at which a growth rate change occurs. Fitting was performed as described in Baumgärtner *et al.*, by fitting two constant functions to the  $i$  initial points and to the  $n-i$  last points<sup>S1</sup>. The  $i^{\text{th}}$  fit with the lowest sum of the squared residuals was chosen (**Supplementary Table 2**).

In order to analyze long trapping events of *B. subtilis* (**Fig. 3** and **Supplementary Fig. 7**) the buoyant mass was fitted to three different models:

-simple linear  $m = at + b$ ;

-simple exponential  $m = A_0 e^{at}$ ;

-bilinear  $m = a_1 t + b_1$  for  $t < t_C$ ;  $m = a_2 t + b_2$  for  $t > t_C$ , where  $t_C$  is the time of the rate change point.

Fits were performed by least square curve fits with MATLAB's *lsqcurvefit* function. The fit parameters results and their standard errors are reported in **Supplementary Table 4**.

**Model Selection Criteria.** Comparison of different curve fittings was done by calculating each of the following model selection criteria:

Adjusted Coefficient of Determination:

$$R^2 = 1 - \frac{n-1}{n-p-1} \frac{RSS}{\sum_i (y_i - \bar{y})^2}$$

Reduced Chi-squared:

$$\chi^2 = \frac{1}{n-p} RSS$$

Akaike information criteria:

$$AIC = n \ln \frac{RSS}{n} + 2p + \frac{2p(p+1)}{n-p+1}$$

Schwarz Bayesian information criteria:

$$SBIC = n \ln \frac{RSS}{n} + p \ln n$$

where  $RSS = \sum_i \frac{1}{\varepsilon_i^2} (y_i - y_{i,f})^2$  is the residual sum of squares,  $y_i$  the  $i^{\text{th}}$  data point,  $\varepsilon_i$  the experimental error of the  $i^{\text{th}}$  data point,  $y_{i,f}$  the  $i^{\text{th}}$  point predicted by the fitted function,  $\bar{y}$  the mean of the data,  $n$  the number of data points,  $p$  the number of parameters of the model. Perfect linear data will have  $R^2 = 1$ ; the lower the  $\chi^2$ ,  $AIC$  and  $SBIC$ , the better the model describes the experimental data<sup>S2</sup>. Calculations were performed in MATLAB.

## Supplementary References

- S1. Baumgartner, S. & Tolic-Norrelykke, I.M., *Biophys. J.*, 96, 4336-47 (2009).
- S2. Buchwald, P. & Sveiczer, A., *Theor Biol Med Model*, 3, 16 (2006).
- S3. Hartwell, L.H. & Unger, M.W., *J Cell Biol*, 75, 422-35 (1977).
- S4. Lord, P.G. & Wheals, A.E., *J Cell Sci*, 50, 361-76 (1981).